


Skyrmion-based magnetic traps for ultracold atoms

Ren Qin and Yong Wang ^{*}

School of Physics, Nankai University, Tianjin 300071, China



(Received 1 January 2020; accepted 29 April 2020; published 19 May 2020)

We show that the stray field generated by isolated magnetic skyrmions can be used to trap ultracold atoms. Especially, ring-shaped and double-well trapping potentials for ultracold atoms can be created by combining the field from two isolated skyrmions. The geometry size, potential barrier, trapping frequency, and Majorana loss rate of these magnetic traps can be tuned by an external magnetic field or device configuration. The results here could be useful to develop atomtronics devices by manipulating magnetic skyrmions with modern spintronics techniques.

DOI: [10.1103/PhysRevA.101.053428](https://doi.org/10.1103/PhysRevA.101.053428)

I. INTRODUCTION

Magnetic traps have been widely exploited to spatially confine and store neutral atoms at extremely low temperatures, which are the key ingredients to investigate ultracold atom physics and design atom-based quantum devices [1,2]. The magnetic fields for traps are usually generated from current-carrying conductive microstructures [1,3,4], permanent magnets with fabricated patterns [2,5]. Alternatively, several schemes have been proposed and realized to trap ultracold atoms with the magnetic field carried by certain topological defects, such as the domain wall in ferromagnetic material [6,7], the vortex in superconductors [8,9], etc. Compared with artificial structures, the magnetic traps based on topological defects can be controlled, reconfigured, and scaled in an easier way.

The experimental discovery of magnetic skyrmions in chiral ferromagnetic materials [10–12] provides another promising opportunity to design magnetic traps for ultracold atoms. The emergence of such kinds of spin texture will significantly affect the stray field distribution near the film surface [13–15]. Depending on the host materials, the size of the magnetic skyrmion can vary from several nanometers to several hundreds nanometers [16–18]. This feature makes it flexible to obtain nanoscale magnetic traps, which is rather difficult for conventional microstructures [1,2]. Furthermore, spintronics techniques to create, control, and eliminate magnetic skyrmions have been well developed nowadays [16–18]. Therefore, skyrmion-based magnetic traps can be easily reconfigured and moved by modern spintronics techniques, which will be advantageous for practical applications. In fact, it has been proposed that several types of magnetic lattices for ultracold atoms can be constructed from the stray field of chiral ferromagnetic films in the skyrmion lattice phase [19].

In this paper, we show that magnetic traps can be constructed from the stray field of isolated magnetic skyrmions. Furthermore, we find that ring-shaped and double-well magnetic traps can be realized by placing two magnetic skyrmions

appropriately. We will also study how to tune the physical properties of these traps by an external magnetic field or device geometry, and discuss their potential applications to develop quantum devices based on ultracold atoms.

II. TRAP WITH SINGLE SKYRMION

Figure 1 demonstrates the basic principle to construct a magnetic trap for ultracold atoms from one isolated magnetic skyrmion. The skyrmion is generated in a chiral ferromagnetic film with thickness d , which will establish the stray field $\mathbf{B}_c(\mathbf{r})$ near the film surface. Recently, this stray field has been measured by nitrogen-vacancy-center-based magnetometry [13] and magnetic force microscopy [14]. A bias magnetic field \mathbf{B}_0 is applied in order to create a zero-field point at finite height. Such a zero-field point is desirable to trap the ultracold atoms prepared at the weak-field seeking state [2]. In addition, a rotating magnetic field $\mathbf{B}_M = B_M[\sin(\omega_M t), \cos(\omega_M t), 0]$ is introduced to suppress the Majorana loss at the zero-field point [9]. Such a configuration will generate a potential $U(\mathbf{r}) = m_F g_F \mu_B B(\mathbf{r})$ for an atom in the hyperfine state $|F, m_F\rangle$. Here, $B(\mathbf{r})$ is the modulus of the total field $\mathbf{B} = \mathbf{B}_c + \mathbf{B}_0 + \mathbf{B}_M$; g_F is the Landé factor, μ_B is the Bohr magneton, F is the total angular momentum quantum number, and m_F is the magnetic quantum number of the atom. This potential can trap the ultracold atoms with a weak-field seeking state ($m_F g_F > 0$) at its minimum point, with the trapping frequency $\omega_T = \sqrt{U''/m_a}$ and the Majorana loss rate $\Gamma/2\pi = \omega_T \exp(-4\omega_L/\omega_T)$ [2,9]. Here, m_a is the mass and ω_L is the Larmor precession frequency of the atom.

The magnetization configuration $\mathbf{m}(\mathbf{r})$ for a single magnetic skyrmion can be obtained by performing microscopic magnetic simulations for a chiral ferromagnetic film, whose energy density functional is defined as [15–19]

$$\mathcal{E}[\mathbf{m}] = \frac{J}{2}(\nabla\mathbf{m})^2 - D\mathbf{m} \cdot (\nabla \times \mathbf{m}) - K\mathbf{m}_z^2 - M_s\mathbf{B}_0 \cdot \mathbf{m}. \quad (1)$$

The four terms in $\mathcal{E}[\mathbf{m}]$ describe the Heisenberg exchange interaction, Dzyaloshinskii-Moriya interaction, perpendicular magnetic anisotropy energy, and Zeeman energy, respectively.

^{*}yongwang@nankai.edu.cn

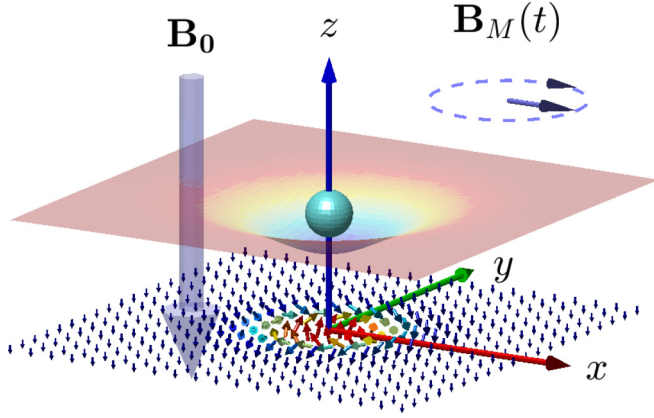


FIG. 1. Schematic diagram for the magnetic trap with a single skyrmion. A chiral ferromagnetic film is placed in the x - y plane with an isolated skyrmion at the origin of coordinates. $\mathbf{B}_0 = (0, 0, -B_0)$ is a bias magnetic field to create a zero-field point at finite height, and $\mathbf{B}_M(t) = B_M[\sin(\omega_M t), \cos(\omega_M t), 0]$ is a rotating magnetic field to suppress the Majorana loss. An ultracold atom is trapped at the minimum point of the magnetic potential.

During all the simulations in this paper, the size of the film is set as $100 \times 100 \times 1 \text{ nm}^3$ and the periodic boundary condition has been exploited. The material parameters are set as $J = 20 \text{ pJ/m}$, $D = 3 \text{ mJ/m}^2$, and $K = 0.7 \text{ MJ/m}^3$. Also, a saturation magnetization $M_s = 580 \text{ kA/m}$ and a Gilbert damping coefficient $\alpha = 0.05$ have been used. Then the profile of an isolated magnetic skyrmion is obtained by relaxing an initial configuration $\mathbf{m}_0(\mathbf{r})$ of the film, where a $21 \times 21 \times 1 \text{ nm}^3$ region in the middle is set as $(0,0,1)$ and the other part as $(0, 0, -1)$. Finally, the spatial distribution of the stray field $\mathbf{B}_c(\mathbf{r})$ is calculated from the magnetization configuration $\mathbf{m}(\mathbf{r})$ as

$$\mathbf{B}_c(\mathbf{r}) = \frac{\mu_0}{4\pi} \int d\mathbf{r}' \frac{3[\mathbf{m}(\mathbf{r}') \cdot \hat{\mathbf{R}}]\hat{\mathbf{R}} - \mathbf{m}(\mathbf{r}')}{R^3}. \quad (2)$$

Here, μ_0 is the vacuum permeability, and $\mathbf{R} = \mathbf{r} - \mathbf{r}'$ denotes the displacement vector between two spatial points.

After setting the skyrmion center as the origin of the coordinates and the chiral ferromagnetic film in the x - y plane, Figs. 2(a) and 2(b) present the distribution of $\mathbf{B}_c(\mathbf{r})$ in the cross-sectional planes $y = 0 \text{ nm}$ and $z = 15 \text{ nm}$ when $\mathbf{B}_0 = \mathbf{0}$. As expected, $\mathbf{B}_c(\mathbf{r})$ is cylindrically symmetric around the z axis and will gradually decay away from the skyrmion. Especially, $\mathbf{B}_c(\mathbf{r})$ on the z axis will be along the z direction. These features can be further understood from an approximate expression of $\mathbf{m}(\mathbf{r}) = (\sin \theta \cos \psi, \sin \theta \sin \psi, \cos \theta)$ in the polar coordinates for the isolated skyrmion [14], where

$$\theta = \pi - \sin^{-1} \left[\tanh \left(\frac{\rho + R}{w} \right) \right] - \sin^{-1} \left[\tanh \left(\frac{\rho - R}{w} \right) \right],$$

$$\psi = \tan^{-1} \left(\frac{y}{x} \right).$$

Here, $\rho = \sqrt{x^2 + y^2}$, and R and w are the radius and thickness of the skyrmion [14]. For the magnetic skyrmion simulated here, we have $R = 8.7 \text{ nm}$ and $w = 3.4 \text{ nm}$. With the dipole approximation [14], the stray field in the cylindrical

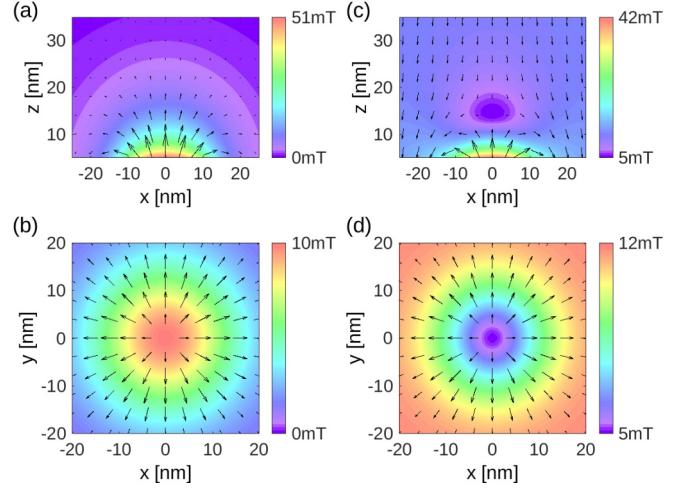


FIG. 2. Magnetic field distributions of the magnetic trap with a single skyrmion. (a) \mathbf{B}_c and its modulus in the x - z plane with $y = 0 \text{ nm}$; (b) \mathbf{B}_c and its modulus in the x - y plane with $z = 15 \text{ nm}$; (c) \mathbf{B} and its modulus in the x - z plane with $y = 0 \text{ nm}$; (d) \mathbf{B} and its modulus in the x - y plane with $z = 15 \text{ nm}$. Here, \mathbf{B}_c is numerically calculated from the microscopic simulation; $B_0 = 10 \text{ mT}$ and $B_M = 5 \text{ mT}$ have been exploited to construct the trap.

coordinates generated by the skyrmion will be

$$B_{c,\rho} = \frac{\mu_0 P}{4\pi} \frac{3\rho z}{(\rho^2 + z^2)^{5/2}}, \quad B_{c,z} = \frac{\mu_0 P}{4\pi} \frac{2z^2 - \rho^2}{(\rho^2 + z^2)^{5/2}},$$

where $\mathbf{P} = P\hat{\mathbf{z}}$ is the magnetic dipole moment of the skyrmion with $P = 2\pi M_s d \int_0^\infty d\rho \rho [1 + \cos \theta(\rho)]$ [14]. When $\rho = 0$, we will get $B_{c,\rho} = 0$ and $B_{c,z} = \frac{\mu_0 P}{2\pi} P z^{-3}$, which coincides with the numerical results in Figs. 2(a) and 2(b) above.

When the bias magnetic field $\mathbf{B}_0 = (0, 0, -B_0)$ is turned on, the zero-field point will be created on the z axis with the height $z_{\min} = \left(\frac{\mu_0 P}{2\pi B_0} \right)^{1/3}$. The application of a rotating magnetic field \mathbf{B}_M will further turn the zero-field point into a nonzero minimum point in the trapping potential $U(r)$. Figures 2(c) and 2(d) show the field distribution in the cross-sectional planes $y = 0 \text{ nm}$ and $z = 15 \text{ nm}$ after setting $B_0 = 10 \text{ mT}$ and $B_M = 5 \text{ mT}$. Thereby, a magnetic trap has been established to trap the ultracold atoms in the weak-field seeking state.

The physical properties of the magnetic trap can be further tuned by the bias magnetic field \mathbf{B}_0 . First, the trapping height z_{\min} will become smaller with a stronger bias field. As shown in Fig. 3(a), z_{\min} extracted from the simulated $U(\mathbf{r})$ will decline from about 40 to 10 nm when B_0 increases from 0.5 to 20 mT, which also agrees well with the analytical results in the dipole approximation. This fact makes it possible to load the cold atoms from an infinite region to the magnetic trap adiabatically [20].

We further estimated the trapping volume V_{eff} for a ^{87}Rb atom in the hyperfine state $|F = 2, m_F = 2\rangle$, which is given as $V_{\text{eff}} = \int e^{-[U(\mathbf{r}) - U(r_{\min})]/k_B T} d\mathbf{r}$ [21]. Here, k_B is the Boltzmann constant and T is the temperature of the ultracold atom. Taking the harmonic approximation for $U(\mathbf{r})$ and setting $k_B T = \hbar \omega_T$, the dependence of V_{eff} on the bias magnetic field is shown in Fig. 3(b). As B_0 increases from 0.5 to 20 mT, V_{eff} will exponentially decay from 10^5 to 10^2 nm^3 . In order to

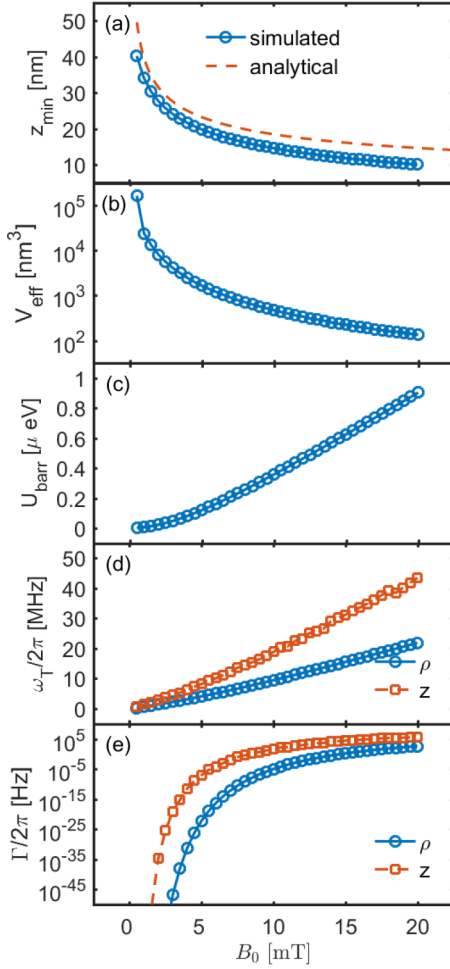


FIG. 3. The dependence of trap parameters on the bias field B_0 for a ^{87}Rb atom in the hyperfine state $|F = 2, m_F = 2\rangle$. (a) Trapping height z_{\min} , which has been obtained from micromagnetic simulation (real line) and from the dipole approximation analytically (dashed line); (b) trapping volume V_{eff} ; (c) trapping barrier U_{barr} ; (d) trapping frequency ω_T ; (e) Majorana loss rate Γ . Here, $B_M = 5$ mT. ρ and z denote the radial and axial components of ω_T and Γ .

capture the atom during the initial loading process, a weak bias magnetic field or larger magnetic skyrmion should be exploited to get a large enough trapping volume.

The trapping barrier U_{barr} , trapping frequency ω_T , and Majorana loss rate Γ of the trap for a ^{87}Rb atom have also been investigated and shown in Figs. 3(c)–3(e). The trapping barrier $U_{\text{barr}} = U(r \rightarrow \infty) - U(r_{\min})$ is the potential for the atoms to overcome. Considering that $B(r \rightarrow \infty) = \sqrt{B_0^2 + B_M^2}$ and $B(r_{\min}) = B_M$, U_{barr} will be irrelevant to the magnetic field \mathbf{B}_c , which vanishes far away from the magnetic skyrmion. As shown in Fig. 3(c), U_{barr} will monotonically increase from 0 to about $1 \mu\text{eV}$ along with an increased bias field B_0 from 0 to 20 mT. Since the trapping potential is cylindrically symmetric around the z axis, there will exist the radial and axial components for both ω_T and Γ . As shown in Figs. 3(d) and 3(e), when the bias field B_0 increases from 0 to 20 mT, $\omega_{T,\rho}/2\pi$ will increase from 0 to about 40 MHz and $\omega_{T,z}/2\pi$ will increase from 0 to about 20 MHz; meanwhile, $\Gamma/2\pi$

will exponentially increase to about 10^5 Hz due to the large trapping frequency. Therefore, a stronger bias field will result in a higher trapping frequency for the trap, but will also cause a larger Majorana loss.

Besides, the Larmor precession frequency at the minimum point will be $\omega_L/2\pi = 70$ MHz for $B_M = 5$ mT. In order to fulfill the time-averaged orbiting potential (TOP) trap condition $\omega_T \ll \omega_M \ll \omega_L$, the bias magnetic field B_0 should be weak enough for a small trap frequency. For example, we have $\omega_{T,\rho}/2\pi = 0.14$ MHz and $\omega_{T,z}/2\pi = 0.79$ MHz when $B_0 = 0.5$ mT, thus we can choose $\omega_M/2\pi = 7$ MHz for the rotating magnetic field \mathbf{B}_M . In fact, the TOP trap condition can be better guaranteed for a larger skyrmion, which will give a smaller field gradient and then lower trapping frequency.

III. RING-SHAPED AND DOUBLE-WELL MAGNETIC TRAPS

In addition to the single-well trap, other types of traps have also been designed and realized for ultracold atoms. Examples include the ring-shaped trap [22–25] for inertial sensors or gyroscopes and a double-well trap [26–28] for matter-wave interferometry. Here, we show how to construct ring-shaped and double-well magnetic traps with two magnetic skyrmions located in two identical chiral ferromagnetic films. These two films are in parallel to the x - y plane and their distance is d . The centers of the two skyrmions are both on the z axis, and the origin of the coordinates is reset in the middle of the two centers. Then the cylindrical symmetry around the z axis will

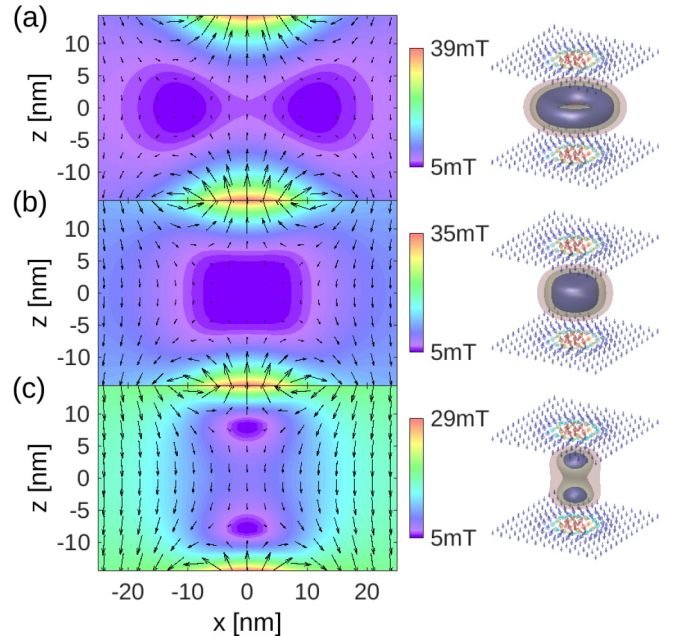


FIG. 4. Magnetic field distributions in the x - z plane with $y = 0$ nm (left) and isosurfaces of field modulus $B(\mathbf{r})$ (right) for three types of magnetic traps formed by two isolated skyrmions. (a) Ring-shaped trap with isosurface values 5.5, 6, and 6.5 mT; (b) intermediate trap with isosurface values 6, 7, and 8 mT; (c) double-well trap with isosurface values 7, 9, and 11 mT. The bias fields B_0 for the three traps are 5, 9, and 15 mT, respectively. The distance d between the two skyrmions is 41 nm, and $B_M = 5$ mT.

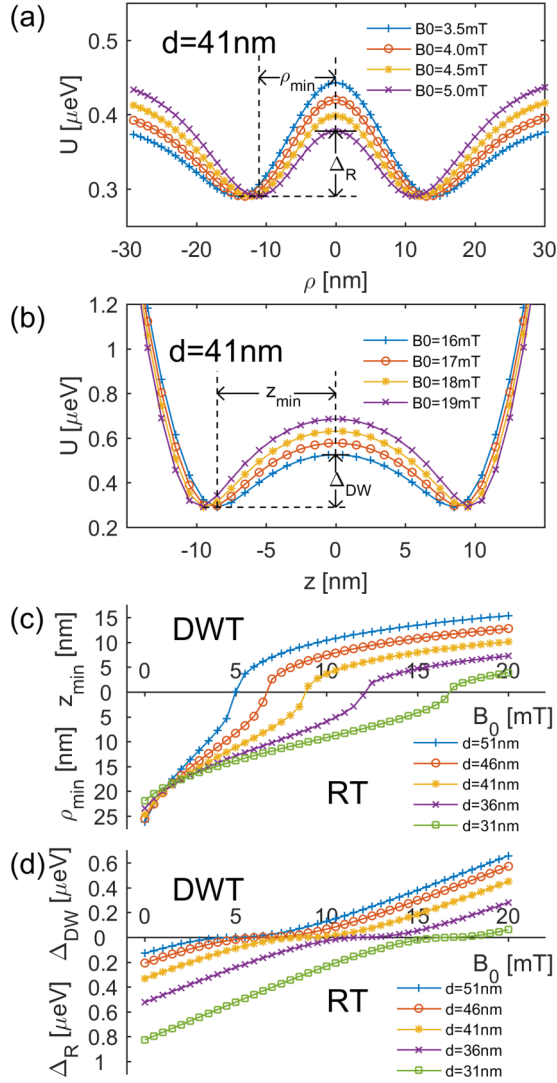


FIG. 5. The dependence of trapping potential $U(\mathbf{r})$ on the bias field B_0 and distance d for a ^{87}Rb atom in the hyperfine state $|F = 2, m_F = 2\rangle$. (a) $U(\rho, z = 0)$ of the ring-shaped trap with fixed $d = 41$ nm and different $B_0 = 3.5, 4, 4.5,$ and 5 mT; (b) $U(\rho = 0, z)$ of the double-well trap with fixed $d = 41$ nm and different $B_0 = 16, 17, 18,$ and 19 mT; (c) B_0 -dependent trap size ρ_{\min} and z_{\min} for different $d = 31, 36, 41, 46,$ and 51 nm; (d) B_0 -dependent potential barrier Δ_R and Δ_{DW} for different $d = 31, 36, 41, 46,$ and 51 nm. RT: ring-shaped trap; DWT: double-well trap.

still be maintained for the stray field \mathbf{B}_c between the two films. Within the dipole approximation, the field distribution in the $z = 0$ plane will be

$$B_{c,\rho}(\rho, z = 0) = 0, \quad B_{c,z}(\rho, z = 0) = \frac{\mu_0 P}{2\pi} \frac{[2(\frac{d}{2})^2 - \rho^2]}{[\rho^2 + (\frac{d}{2})^2]^{\frac{5}{2}}},$$

while in the z axis, one has

$$B_{c,\rho}(\rho = 0, z) = 0, \quad B_{c,z}(\rho = 0, z) = \frac{\mu_0 P}{\pi} \frac{[(\frac{d}{2})^3 + 3(\frac{d}{2})z^2]}{[(\frac{d}{2})^2 - z^2]^{\frac{5}{2}}}.$$

Obviously, the zero-field points of \mathbf{B}_c will form a ring with the radius $\rho_{\min} = \frac{d}{\sqrt{2}}$ in the $z = 0$ plane if no bias magnetic

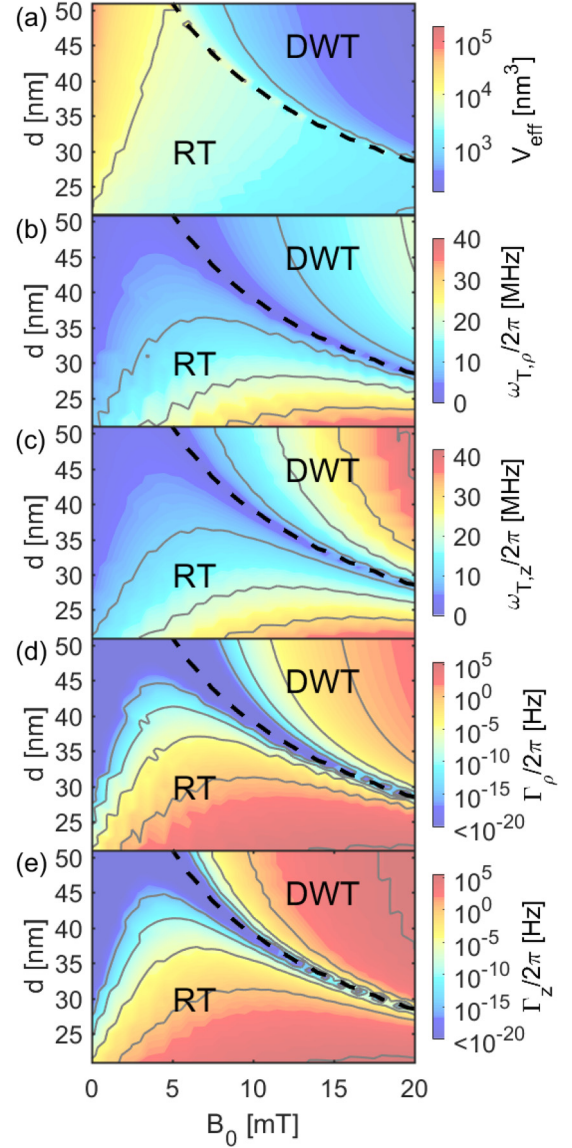


FIG. 6. The dependence of trapping volume V_{eff} , trapping frequency ω_T , and Majorana loss rate Γ on the bias field B_0 and distance d for a ^{87}Rb atom in the hyperfine state $|F = 2, m_F = 2\rangle$. (a) Trapping volume V_{eff} ; (b) radial component of ω_T ; (c) axial component of ω_T ; (d) radial component of Γ ; (e) axial component of Γ . RT: ring-shaped trap; DWT: double-well trap. The black dashed curve denotes the parameters to form the intermediate traps.

field is applied. Therefore, the ultracold atoms in the weak-field seeking state can be trapped in a ring-shaped potential in this case. However, if a bias magnetic field $\mathbf{B}_0 = (0, 0, -B_0)$ is present, the radius ρ_{\min} of the ring will expand if $B_0 < 0$ and shrink if $B_0 > 0$. In particular, the ring will shrink into a point at the critical value $B_0 = \frac{8\mu_0 P}{\pi d^3}$, where the ring-shaped trap will become a single magnetic trap. Furthermore, if $B_0 > \frac{\mu_0 8P}{\pi d^3}$, two zero-field points will symmetrically appear at $\pm z_{\min}$ on the z axis, which can be used to construct a double-well magnetic trap for cold atoms.

The deduction above is confirmed by the spatial distribution of magnetic field between two chiral ferromagnetic films based on a micromagnetic simulation. The same material

TABLE I. Configurations and parameters of three types of magnetic traps for a ^{87}Rb atom, i.e., single-well trap (SWT), ring-shaped trap (RT), and double-well trap (DWT). Magnetic skyrmions with two different geometry sizes have been exploited to construct the traps, where the micromagnetic parameters J, D, K in units (pJ/m, mJ/m², MJ/m³) are set as (20,3,0.7) and (8000,60,0.7), respectively. Here, we have presented the radius R and thickness w of the skyrmion, the distance d between two skyrmions (for RT and DWT only), the magnetic field B_0 and B_M , the TOP rotating frequency ω_M , the Larmor precessing frequency ω_L , the trapping frequency ω_T , the Majorana loss rate Γ , the effective trapping volume V_{eff} , and the trapping depth.

Trap type	Trap configuration						Trap parameters					
	R (nm)	w (nm)	d (nm)	B_0 (mT)	B_M (mT)	$\omega_M/2\pi$ (MHz)	$\omega_{T,\rho}/2\pi$ (MHz)	$\omega_{T,z}/2\pi$ (MHz)	$\omega_L/2\pi$ (MHz)	$\Gamma/2\pi$ (MHz)	V_{eff} (nm ³)	Depth (mK)
SWT	8.7	3.4		2	5	7	1.43	2.89	70.0	$<10^{-41}$	8.1×10^3	0.26
	165.3	68.1		10	20	7	0.24	0.47	279.8	$<10^{-100}$	1.2×10^5	1.58
RT	8.7	3.4	51	2	5	10	3.21	3.24	70.0	$<10^{-36}$	2.2×10^4	0.26
	165.3	68.1	600	10	20	10	0.42	0.42	279.8	$<10^{-100}$	1.0×10^5	1.58
DWT	8.7	3.4	51	7	5	10	4.23	8.61	70	$<10^{-12}$	1.5×10^3	2.42
	165.3	68.1	1020	10	20	10	0.20	0.42	279.8	$<10^{-100}$	1.5×10^5	1.58

parameters in the previous section have been exploited and the distance of the two films is $d = 41$ nm. A rotating magnetic field with $B_M = 5$ mT is also included. As an example, Fig. 4(a) displays the field distribution in the cross-sectional plane $y = 0$ nm for a ring-shaped trap, where the bias field is $B_0 = 5$ mT. When B_0 is increased to 9 mT, the ring-shaped trap becomes a single magnetic trap centered at the origin with its field distribution in Fig. 4(b). This single magnetic trap will then be split into the double-well trap for a larger bias field, and the case for $B_0 = 15$ mT is given in Fig. 4(c).

The evolution of the magnetic potential $U(\mathbf{r})$ under the bias field B_0 is further calculated for a ^{87}Rb atom in the hyperfine state $|F = 2, m_F = 2\rangle$. For given $d = 41$ nm, Fig. 5(a) shows $U(\rho, z = 0)$ for the ring-shaped traps with $B_0 = 3.5, 4.0, 4.5,$ and 5.0 mT, while Fig. 5(a) shows $U(z, \rho = 0)$ for the double-well traps with $B_0 = 16, 17, 18,$ and 19 mT. The results show that the order of magnitude of $U(\mathbf{r})$ will be tenths of μeV , which corresponds the temperature at the level of mK. Moreover, the ring-shaped trap and double-well trap are characterized by the size $\rho_{\text{min}}, z_{\text{min}}$ and the potential barrier $\Delta_R, \Delta_{\text{DW}}$, and their dependence on the bias field B_0 and the distance d are given in Figs. 5(c) and 5(d), respectively. For fixed d , r_{min} will continuously reduce to zero and then z_{min} will monotonically increase from zero when B_0 is continuously increased from 0 to 20 mT, which coincides with the analytical results above. Besides, the critical values of bias field where $r_{\text{min}} = z_{\text{min}} = 0$ will become larger for a smaller distance d . Therefore, it is also possible to switch the ring-shaped and double-well magnetic traps by tuning the distance d for fixed B_0 . On the other hand, Δ_R will continuously decrease when the ring-shaped trap is shrunk, while Δ_{DW} will monotonically increase with the increased bias field. This fact can be further understood from the strength of the total magnetic field at the origin, where $B(\mathbf{r} = 0) = \sqrt{(\frac{8\mu_0 P}{\pi d^3} - B_0)^2 + B_M^2}$ under the dipole approximation. At the critical field $B_0 = \frac{8\mu_0 P}{\pi d^3}$, one has $B(\mathbf{r} = 0) = B_M$ and the potential barrier will vanish.

Figure 6 displays the trapping volume V_{eff} , trapping frequency ω_T , and Majorana loss rate Γ of the magnetic traps for a ^{87}Rb atom in the B_0 - d parameter plane, which is divided into two regions for the ring-shaped trap and double-well trap by a critical curve for the single trap. The ring-shaped

trap will in general have a larger V_{eff} than the double-well trap, and a larger bias magnetic field B_0 will give a smaller V_{eff} [Fig. 6(a)]. Furthermore, high ω_T can be achieved by increasing the bias field B_0 and decreasing the layer distance d for the ring-shaped trap, while for the double-well trap, both large B_0 and d will result in high ω_T [Figs. 6(b) and 6(c)]. On the other hand, ω_T will drastically decrease in the region around the critical curve or the line $B_0 = 0$ due to the loose trapping potential. Meanwhile, the Majorana loss rate will follow the same trend as the trapping frequency. As shown in Figs. 6(d) and 6(e), $\Gamma/2\pi$ can vary from less than 0 to 10^5 Hz when $\omega_T/2\pi$ increases from 0 to about 40 MHz. The results here suggest that relatively high trapping frequency (~ 1 MHz) with a sufficiently low Majorana loss rate (~ 1 Hz) can be realized for both the ring-shaped and double-well magnetic traps. Considering that the Larmor precessing frequency $\omega_L/2\pi = 70$ MHz for $B_M = 5$ mT, we can set $\omega_M/2\pi = 10$ MHz to fulfill the TOP trap condition.

IV. DISCUSSION AND CONCLUSION

We emphasize that the configurations of the magnetic traps proposed here should be elaborately designed for their practical performance. For example, a large bias magnetic field B_0 is usually necessary for a large trapping depth; however, this will make the trapping volume small. The dilemma will become obvious if the skyrmion size is small, as shown in Table I. For the traps based on smaller skyrmions with radius $R = 8.7$ nm, the effective trapping volumes V_{eff} will be only 10^3 - 10^4 nm³ in order to make the trapping depth around 1 mK. The difficulty will be significantly overcome after exploiting larger skyrmions with $R = 165.3$ nm, where V_{eff} will have the order of magnitude 10^5 nm³ with an even larger trapping depth. Therefore, we expect that the proposed magnetic traps here can be more easily realized with larger magnetic skyrmions.

In conclusion, we show that the stray field of isolated magnetic skyrmions in chiral ferromagnetic films can be utilized to design magnetic traps for ultracold atoms. Single-well trap, ring-shaped, and double-well traps with a high trapping frequency and low Majorana loss rate can be realized by reasonably choosing the material

parameters, device geometry, and external magnetic field. Considering that the magnetic skyrmion is topologically stable and can be flexibly manipulated by modern spintronics techniques, the strategy proposed here could be advantageous to integrate skyrmion-based magnetic traps into atomtronics devices.

ACKNOWLEDGMENTS

This work has been supported by NSFC Projects No. 61674083 and No. 11604162 and by the Fundamental Research Funds for the Central Universities, Nankai University (Grant No. 7540).

-
- [1] J. Fortágh and C. Zimmermann, *Rev. Mod. Phys.* **79**, 235 (2007).
- [2] *Atom Chips*, edited by J. Reichel and V. Vuletić (Wiley-VCH, Berlin, 2011).
- [3] J. Reichel, W. Hänsel, and T. W. Hänsch, *Phys. Rev. Lett.* **83**, 3398 (1999).
- [4] R. Folman, P. Krüger, D. Cassettari, B. Hessmo, T. Maier, and J. Schmiedmayer, *Phys. Rev. Lett.* **84**, 4749 (2000).
- [5] A. L. La Rooij, H. B. van Linden van den Heuvell, and R. J. C. Spreeuw, *Phys. Rev. A* **99**, 022303 (2019).
- [6] D. A. Allwood, T. Schrefl, G. Hrkac, I. G. Hughes, and C. S. Adams, *Appl. Phys. Lett.* **89**, 014102 (2006).
- [7] A. D. West, K. J. Weatherill, T. J. Hayward, P. W. Fry, T. Schref, M. R. J. Gibbs, C. S. Adams, D. A. Allwood, and I. G. Hughes, *Nano. Lett.* **12**, 4065 (2012).
- [8] T. Müller, B. Zhang, R. Fermani, K. S. Chan, Z. W. Wang, C. B. Zhang, M. J. Lim, and R. Dumke, *New J. Phys.* **12**, 043016 (2010).
- [9] O. Romero-Isart, C. Navau, A. Sanchez, P. Zoller, and J. I. Cirac, *Phys. Rev. Lett.* **111**, 145304 (2013).
- [10] U. K. Röbler, A. N. Bogdanov, and C. Pfleiderer, *Nature (London)* **442**, 797 (2006).
- [11] S. Mühlbauer, B. Binz, F. Jonietz, C. Pfleiderer, A. Rosch, A. Neubauer, R. Georgii, and P. Böni, *Science* **323**, 915 (2009).
- [12] X. Z. Yu, Y. Onose, N. Kanazawa, J. H. Park, J. H. Han, Y. Matsui, N. Nagaosa, and Y. Tokura, *Nature (London)* **465**, 901 (2010).
- [13] Y. Dovzhenko, F. Casola, S. Schlotter, G. S. D. Beach, and A. Yacoby, *Nat. Commun.* **9**, 2712 (2018).
- [14] A. Yagil, A. Almoalem, A. Soumyanarayanan, A. K. C. Tan, M. Raju, C. Panagopoulos, and O. M. Auslaender, *Appl. Phys. Lett.* **112**, 192403 (2018).
- [15] R. Qin and Y. Wang, *New J. Phys.* **20**, 063029 (2018).
- [16] N. Nagaosa and Y. Tokura, *Nat. Nanotechnol.* **8**, 899 (2013).
- [17] R. Wiesendanger, *Nat. Rev. Mater.* **1**, 16044 (2016).
- [18] A. Fert, N. Reyren, and V. Cros, *Nat. Rev. Mater.* **2**, 17031 (2017).
- [19] R. Qin and Y. Wang, *Phys. Rev. A* **99**, 013401 (2019).
- [20] D. M. Stamper-Kurn, H.-J. Miesner, A. P. Chikkatur, S. Inouye, J. Stenger, and W. Ketterle, *Phys. Rev. Lett.* **81**, 2194 (1998).
- [21] J. Pérez-Ríos and A. S. Sanz, *Am. J. Phys.* **81**, 836 (2013).
- [22] J. A. Sauer, M. D. Barrett, and M. S. Chapman, *Phys. Rev. Lett.* **87**, 270401 (2001).
- [23] S. Gupta, K. W. Murch, K. L. Moore, T. P. Purdy, and D. M. Stamper-Kurn, *Phys. Rev. Lett.* **95**, 143201 (2005).
- [24] O. Morizot, Y. Colombe, V. Lorent, H. Perrin, and B. M. Garraway, *Phys. Rev. A* **74**, 023617 (2006).
- [25] W. H. Heathcote, E. Nugent, B. T. Sheard, and C. J. Foot, *New J. Phys.* **10**, 043012 (2008).
- [26] W. Hänsel, J. Reichel, P. Hommelhoff, and T. W. Hänsch, *Phys. Rev. A* **64**, 063607 (2001).
- [27] Y. Shin, M. Saba, A. Schirotzek, T. A. Pasquini, A. E. Leanhardt, D. E. Pritchard, and W. Ketterle, *Phys. Rev. Lett.* **92**, 150401 (2004).
- [28] T. Schumm, S. Hofferberth, L. M. Andersson, S. Wildermuth, S. Groth, I. Bar-Joseph, J. Schmiedmayer, and P. Krüger, *Nat. Phys.* **1**, 57 (2005).